Available online at www.sciencedirect.com
SCIENCE DIRECT®
Nuclear Instruments and Methods in Physics Research A 554 (2005) 75–84
NUCLEAR INSTRUMENTS & METHODS IN PHYSICS RESEARCH Section A
www.elsevier.com/locate/nima

Polarimetry of coherent bremsstrahlung by analysis of the photon energy spectrum

S. Darbinyan[a], H. Hakobyan[a,*], R. Jones[b], A. Sirunyan[a], H. Vartapetian[a]

[a]*EPD, Yerevan Physics Institute, Alikhanian Brother str., 375036 Yerevan, Armenia*
[b]*University of Connecticut, Storrs, CT, USA*

Received 8 August 2005; accepted 9 August 2005
Available online 26 August 2005

Abstract

A method of coherent bremsstrahlung (CB) polarimetry based on the analysis of the shape of the photon energy spectrum is presented. The influence of a number of uncertainty sources, including the choice of atomic form-factors, has been analyzed. For a CB source consisting of a diamond radiator and multi-GeV electrons, an absolute accuracy of polarimetry at the level of 0.01–0.02 is attainable.

PACS: 14.70.Bh; 24.70.+s; 78.70.−g

Keywords: Coherent bremmstrahlung; Linear polarization; Polarimetry

1. Introduction

Coherent bremsstrahlung (CB) of electrons in a crystal radiator is a well-known method for the production of intense, linearly polarized photon beams in the range of intermediate and high energies [1]. The availability of a GeV-scale electron beams with steadily increasing quality and intensity has created opportunities for experiments that exploit secondary beams of polarized photons generated using the CB technique (see, for example, Ref. [2] and references therein). Together with the improvements in the intensity and quality of the CB beam has come increasingly stringent requirements on the degree of polarization of the beam and, in particular, on how well the polarization is known. Beginning with the experimental discovery of the CB process in the 1960s, the polarization of the coherent radiation was calculated based on the known theoretical correlation between the CB intensity and polarization spectra [3]. By this approach, the task of polarimetry becomes the task of understanding and fitting the shape of the bremsstrahlung photon

*Corresponding author. Tel.: +3741 355093; fax: +3741 398392.
E-mail address: hakopian@mail.cern.ch (H. Hakobyan).

0168-9002/$ - see front matter © 2005 Elsevier B.V. All rights reserved.
doi:10.1016/j.nima.2005.08.039

energy spectrum, which is known as CB shape analysis (CBSA).

A very few direct and precise measurements of CB polarization had been done, exploiting electromagnetic or nuclear processes. The earliest of them was carried out at DESY [4] for a CB peak energy of 2.05 GeV by means of an azimuthal asymmetry measurement of the e^+e^- coherent pair production in a diamond crystal. The data obtained established a fairly good agreement between the measured polarization and that inferred using a CBSA method, although no measure of quantitative agreement was extracted.

Polarization data, recently measured at the CB peak energy of 300 MeV using the analyzing power of coherent π^0 production on a ^{4}He target [5] are also in good agreement with CBSA calculations, however, without stating the uncertainty on the CBSA result which appears to be on the order of 0.02–0.03 or better.

The use of nuclear reactions for CB polarimetry is mainly restricted by the rapid decrease of the coherent nuclear photoproduction cross-sections with a photon energy, as compared to accompanying incoherent processes.

Pushing the precision of CB polarimetry towards the percent level will require a combination of direct polarimetry measurements and CBSA, together with a quantitative understanding of the uncertainties of each. Even in the presence of a polarimeter with a known analyzing power, a cross-check using a CBSA method is essential for substantiating a claim of 1–2% absolute polarization uncertainty. The CBSA method also provides a continuous monitor of the polarization during regular data collection periods, unlike direct methods which generally require the interruption of regular data collection for dedicated polarimetry runs. CBSA relies only on data from the tagging spectrometer, without requiring any additional detector hardware or electronics than is essential to the operation of any tagged bremsstrahlung source.

In this paper we present and discuss a specific approach to CBSA that has been developed at YERPHI, and show how this method can reach a level of accuracy that is required for it to serve as a precise polarimetry method as well as an effective cross-check of direct polarimetry measurements at the level of 1–2%.

2. CB shape analysis methods

The CB intensity spectrum and polarization arising from 4.5 GeV electrons incident on a diamond crystal in a direction close to the [1 0 0] axis are shown in Fig. 1. The kinematics of the bremsstrahlung process are shown in the inset Fig. 1(a), where angles θ and α define the incident electron momentum vector within the right-handed coordinate system formed by the three principal crystal axes of the diamond lattice $(\vec{b_2}, \vec{b_3}, \vec{b_1})$. Panels (b) and (c) show the CB photon intensity and polarization spectra, respectively, for a crystal orientation that places the primary coherent edge of the reciprocal lattice vector $(0\,\bar{2}\,2)$ at 1.3 GeV. The secondary peaks appearing at simple multiples of the primary peak energy arise from higher-order recurrences of the lattice vector $(0\,\bar{2}\,2)$, while contributions from other lattice vectors appear superimposed upon each other in the region of the end point. The solid curves in Fig. 1 represent the theoretical intensity and polarization spectra under the assumption of a perfect crystal, perfect beam, and perfect resolution. The dashed curves represent the deformation of the actual measured spectra from the ideal case, after realistic experimental conditions are taken into account. Analytical expressions for the CB intensity and polarization are presented in Appendix A. One important thing to note in Fig. 1 is that, even though a single lattice vector may dominate in the vicinity of a peak in the intensity spectrum, contributions from the tails of all higher-lying peaks are also present and must be taken into account.

CBSA methods generally use a fit of the measured CB spectrum to the convolution of the theoretical intensity I^{th} $((x, \theta, \alpha))$ with a smearing function $W(\theta, \alpha)$ according to the equation

$$I^{\mathrm{exp}}(x) = \int I^{\mathrm{th}}(x, \theta, \alpha)\, W(\theta, \alpha)\, \mathrm{d}\theta\, \mathrm{d}\alpha \qquad (1)$$

where $x = E_\gamma / E_e$ is a relative energy of the radiated photon and $W(\theta, \alpha)$ describes the influence of

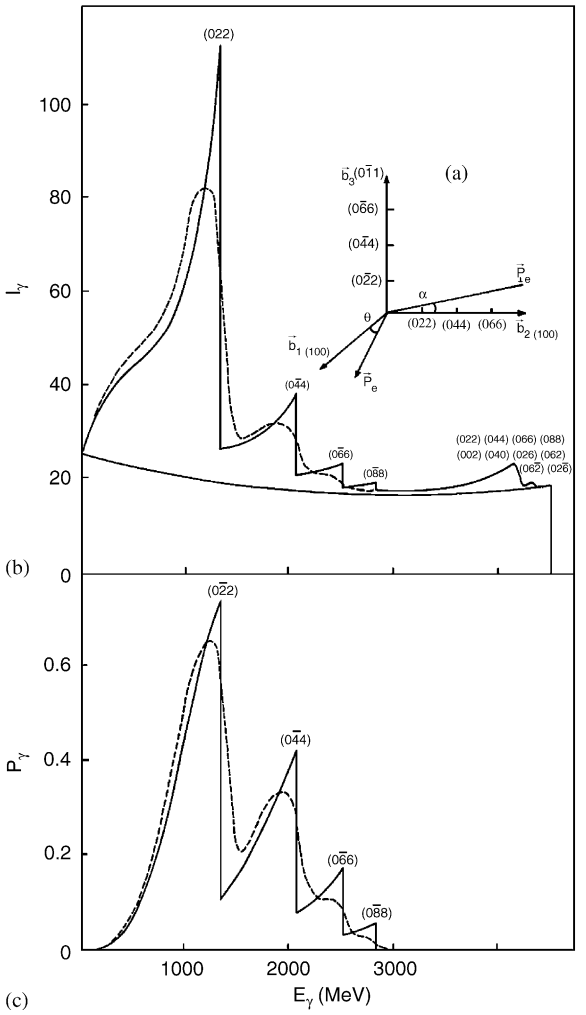

Fig. 1. (a) Orientation of the primary electron momentum relative to the crystallographic axes of the diamond lattice. (b, c) The sample of the theoretical spectra of the intensity and polarization (full curves) and the Monte-Carlo-simulated ones (dashed curves), illustrating the influence of the experimental smearing factors.

different experimental factors on a CB spectral shape, such as are an angular divergence of the primary electrons, collimation of the secondary photons, multiple scattering and imperfections of the crystal, energy resolution of the experimental setup, etc.

The smearing function is parameterized in an analytical form involving several free parameters that are adjusted during the fitting procedure. Once the function $W(\theta,\alpha)$ has been fixed, the polarization spectrum is determined according to the expression

$$P^{\exp}(x) = \int P^{\mathrm{th}}(x,\theta,\alpha)\, I^{\mathrm{th}}(x,\theta,\alpha) \times W(\theta,\alpha)\,\mathrm{d}\theta\,\mathrm{d}\alpha / I^{\exp}(x) \quad (2)$$

or

$$P^{\exp}(x) = \int 2(1-x)\psi_3^{\mathrm{c}}(x,\theta,\alpha) \times W(\theta,\alpha)\,\mathrm{d}\theta\,\mathrm{d}\alpha / I^{\exp}(x) \quad (3)$$

that follows from the definitions of the CB polarization [6,7] (see details in Appendices A and B).

The quality of the fit to the intensity spectra and therefore the accuracy of the parameters is determined by the correctness of the smearing model expressed by the analytical form of the function $W(\theta,\alpha)$ and, with an appropriate choice, can attain the level required to extract the polarization $P^{\exp}$ with a precision of 0.01–0.02 [8,9]. Uncontrolled experimental factors such as an unpredictable beam angular structure or crystal radiation damage can modify the theoretical functions $P^{\mathrm{th}}(x,\theta,\alpha)$ and $I^{\mathrm{th}}(x,\theta,\alpha)$ so that is not possible to describe these distortions in a simple analytical form of $W(\theta,\alpha)$ to obtain a good fit to the intensity spectra. Achieving a good fit, however, is not sufficient in itself to demonstrate an absolute precision on $P^{\exp}$ at that order because $W(\theta,\alpha)$ is not the only source of error in Eq. (2). The choice of the atomic form factor (AFF) that appears in the function $I^{\mathrm{th}}(x,\theta,\alpha)$ can introduce systematic errors of theoretical origin. We have verified the achievable polarimetry precision and corresponding impact of the relevant systematic uncertainties using the methods presented below.

3. Method 1

Method 1 employs the Fourier convolution theorem to extract the experimental smearing function W from the measured and theoretical intensity spectra [8]. The idea is based on an assumption that all experimental factors, which

work to smooth out the sharp features seen in the theoretical spectra can formally be represented by a function which describes the distribution of the measured CB photon energy about its ideal theoretical value. Thus, Eq. (1) can be rewritten as

$$I^{\exp}(x_0) = \int I^{\mathrm{th}}(x)_{\theta,\alpha} W(x - x_0)\,\mathrm{d}x \tag{4}$$

where $I^{\mathrm{th}}(x)_{\theta,\alpha} = I^{\mathrm{th}}(x,\theta,\alpha)$ is defined as the theoretical intensity spectrum for fixed values of a crystal angles (θ,α).

The validity of this idea rests upon a general feature of the theoretical functions $I^{\mathrm{th}}(x,\theta,\alpha)$ and $P^{\mathrm{th}}(x,\theta,\alpha)$ that their dependence upon the crystal orientation angles θ and α is principally through the value that they imply for the high-energy edge of the primary coherent peak (see Fig. 1). That is, for small changes in θ and α, the principal effect on $I^{\mathrm{th}}(x,\theta,\alpha)$ and $P^{\mathrm{th}}(x,\theta,\alpha)$ is simply to shift the coherent peak by a small amount Δx. Thus, the smearing over θ and α that arises from the small divergence of the electron beam and multiple-scattering effects can effectively be described by a convolution of the ideal theoretical spectra with a sharply peaked empirical function $W(\Delta x)$.

Similarly, Eq. (2) can be rewritten as

$$P^{\exp}(x_0) = \int P^{\mathrm{th}}(x)_{\theta,\alpha} I^{\mathrm{th}}(x)_{\theta,\alpha} \times W(x - x_0)\,\mathrm{d}x / I^{\exp}(x_0). \tag{5}$$

Expression (4) is classified as Fredholm's integral equation of the first type with the kernel $W(x - x_0)$ depending only on the difference of the arguments and may be solved by means of Fourier transforms [10]. Carrying out a Fourier transform of both sides of Eq. (4) the Fourier spectrum of the smearing function is given by

$$\tilde{W}(k) = (\tilde{I}^{\exp}(k)/\tilde{I}^{\mathrm{th}}(k))/\sqrt{2\pi} \tag{6}$$

where $\tilde{I}^{\exp}(k), \tilde{I}^{\mathrm{th}}(k)$ are the Fourier spectra of $I^{\exp}(x)$ and $I^{\mathrm{th}}(x)$, respectively. Using the inverse Fourier transformation one can reconstruct $W(x)$.

Substituting the expression for $W(x)$ into Eq. (4) one may obtain the polarization spectrum:

$$P^{\exp}(x) = F^{-1}[\widetilde{P(k)}\tilde{I}^{\exp}(k)]/I^{\exp}(x) \tag{7}$$

where $\widetilde{PI}(k)$ is the Fourier spectrum of the product $P^{\mathrm{th}}(x)I^{\mathrm{th}}(x)$.

As can be seen, a final expression (7) uses the Fourier decomposition amplitudes of the experimental and theoretical spectra only. There is no need of other information, which is a visible advantage of this approach.

4. Method 2

Method 2 is based upon the complete theoretical expression for $P^{\mathrm{th}}(x,\theta,\alpha)$ (see Eq. (A.9)), supplemented with two corrections. The first one consists in replacement of the ratio of coherent to incoherent intensity $I^{\mathrm{coh}}(x,\theta,\alpha)/I^{\mathrm{inc}}(x)$ by its experimental value $\beta^{\exp} = I^{\mathrm{cexp}}(x)/I^{\mathrm{inc.exp}}(x)$ [11] to account for the possible inconsistence between the incoherent component in theoretical and experimental spectra and the presence of extended tails on the smearing functions (see Fig. 1):

$$P(x,\theta,\alpha) = \frac{2(1-x)\psi_3^{\mathrm{c}}(x,\theta,\alpha)}{I^{\mathrm{coh}}(x,\theta,\alpha)} \frac{\beta^{\exp}}{\beta^{\exp}+1} \tag{8}$$

where $I^{\mathrm{cexp}}(x)$ and $I^{\mathrm{coh}}(x)$ are the normalized coherent intensities of the experimental and theoretical spectra. The second correction arises from the need to account for the relatively strong smearing of $(0\,\bar{2}\,2)$ lattice vector contribution to a coherent intensity as compared to the weakly distorted tails from higher-order lattice vector recurrences $0\,\bar{4}\,4$, $0\,\bar{6}\,6$, $0\,\bar{8}\,8$ and others whose contribution is peaking at the high-energy end of the CB intensity spectrum. The correction factor is defined as

$$C(x) = 1 + (I^{\mathrm{cexp}}(x) - I^{\mathrm{coh}}(x))/I_1^{\mathrm{coh}}(x) \tag{9}$$

where $I_1^{\mathrm{coh}}(x)$ is the theoretical contribution of the $0\,\bar{2}\,2$ lattice vector. The factor $C(x)$ is introduced into the expressions for the shape functions (see Eqs. (A.5), (A.6) and (A.8)) as a weight of the $0\,\bar{2}\,2$ lattice vector.

The polarization in the vicinity of the primary coherent peak is dominated by diminishing contributions of the series $0\,\bar{2}\,2$, $0\,\bar{4}\,4$, $0\,\bar{6}\,6$, $0\,\bar{8}\,8$, while the tails of the peaks appearing at the end of the CB spectra give practically non-polarized contribution at the intermediate x region and may be neglected in ψ_3^{c} (Eq. (A.8)). With these

modifications, the expression given in Eq. (8) is used for computing the polarization.

5. Scheme of methods tests

First of all the methods presented above were examined using a variety of the Monte-Carlo (MC) simulated CB spectra for primary peak energies ($x_{(0\,\bar{2}\,2)} = 0.2 - 0.5$), for the conditions of the γ-2 beam line of a YERPHI's electron synchrotron ($E_e = 4.5\,\mathrm{GeV}$, diamond crystal thickness 72 μm, beam effective divergence app. 0.1 mrad, collimation 0.15 mrad (half-aperture). In addition, CB spectra with higher degrees of distortion were generated (collimation 0.3 mrad, average beam divergence 0.3–0.5 mrad) in order to provide more discriminating tests of the CBSA methods presented.

As a first step, the coherent theoretical spectrum has to be constructed corresponding with a given experimental spectrum according to the expression for $I^{\mathrm{th}}(x, \theta, \alpha)$ (see Eqs. (A.1)–(A.8)). The choice of a crystal azimuthal angle α (θ is fixed to a 0.05 rad) is defined by the energy of the $(0\,\bar{2}\,2)$ discontinuity in the theoretical spectrum and may be approximated by the midpoint of the sloping right-hand edge of the peak in the experimental intensity spectrum (Fig. 1b). It is worth mentioning that special care must be taken in the construction of the theoretical spectrum for the case where strong photon beam collimation ($\theta_k < m/E_0$) is applied, in order to correctly include the contributions from all reciprocal lattice vectors that satisfy the known selection criteria [1].

The second step consists of the evaluation and subtraction of a possible incoherent contamination in the CB spectrum. Some level of incoherent contamination is generally present under realistic experimental conditions, in addition to the intrinsic incoherent component in the CB spectrum itself. Possible sources of this contamination include interactions of the tails of the electron beam in the crystal mount material, tails of the electron beam angular distribution, disoriented inclusions in the diamond crystal, and crystal radiation damage. The subtraction procedure is based on the assumption that the experimental effects which smear the theoretical spectrum to produce the experimental one do not appreciably affect the coherent integral over a wide region of the spectrum, so that the integrals of $I^{\mathrm{exp}}(x)$ and $I^{\mathrm{th}}(x)$ should be the same. Using this assumption it is possible to remove the incoherent contamination from the measured spectrum by subtracting the incoherent bremsstrahlung spectrum of standard shape rescaled such that the integrals of $I^{\mathrm{exp}}(x)$ and $I^{\mathrm{th}}(x)$ are equal. As in the Monte-Carlo simulations we used a full screening case [1] for incoherent structure functions. To fix the normalization of the experimental and theoretical spectra, it is convenient to form ratios of spectral integrals and compare them, rather than comparing the integrals directly. For this purpose, two regions of the CB spectrum are chosen for integration, the first being the region around the primary peak $x_{\min} < x < x_{0\,\bar{6}\,6}$) and the second being the plateau region ($0.65 < x < 0.8$ in Fig. 1b). The coherent component dominates in the first region, whereas it contributes only 10–20% in the plateau, so that the above-mentioned ratio has good sensitivity to a small incoherent contamination The region of the peaks associated with lattice vectors $(0\,\bar{2}\,2)$, $(0\,\bar{4}\,4)$ and $(0\,\bar{6}\,6)$ in Fig. 1b is visibly distorted by smearing effects and so is included in the subsequent Fourier analysis, while the flat regions are only weakly distorted and do not contain significant information for this purpose.

Once the incoherent contamination has been removed, the relation between the experimental and theoretical intensity spectra, in analogy with Eq. (4), is replaced by

$$I^{\mathrm{cexp}}(x_0) = \int I^{\mathrm{coh}}(x)_{\theta,\alpha} W_{\mathrm{c}}(x - x_0)\,\mathrm{d}x \tag{10}$$

where $I^{\mathrm{cexp}}, I^{\mathrm{coh}}$ are the coherent intensities of the experimental and theoretical spectra and it is assumed that the function $W_(x - x_0)$ is the same function as that in Eq. (4).

The Fourier transform was realized by means of the Fast Fourier Transform (FFT) algorithm [12] which requires $N = 2^n$ point in the function discrete presentation. Our choice of $N = 64$ spans the region of the $(0\,\bar{2}\,2)$, $(0\,\bar{4}\,4)$, $(0\,\bar{6}\,6)$ peaks. Before submitting a function to Fourier analysis, a statistical smoothing procedure was applied within

the region of interest, which helped to control the generation of large but statistically insignificant high-frequency components in the decomposition spectra. These procedures have been repeated for seven types of AFFs in order to study the influence of the form-factors on the extracted polarization.

6. Results and discussion

The MC-simulated CB spectra for $I^{\exp}(x)$ and $P^{\exp}(x)$ and the corresponding results for polarization obtained with methods 1 and 2 are shown for different peak energies in Figs. 2–4. A good agreement is seen between MC and the results from method 1 with an accuracy $\Delta P = 0.01$ in the region of $\Delta x/x \leqslant 0.6$, reaching 0.02 at the flat ends which are weakly distorted by the smearing factors and have low significance in terms of figure of Merit (IP^2).

The results from method 2 agree as a whole satisfactorily with MC. The agreement is good above the primary peak energies $x \geqslant 0.3$ and even better than for method 1 on the left-hand side of the primary peak. The agreement is somewhat worse at low values of x when the crystal angle α becomes comparable to the smearing angle $\Delta\alpha$ (see Fig. 2). Even there, however, the observed

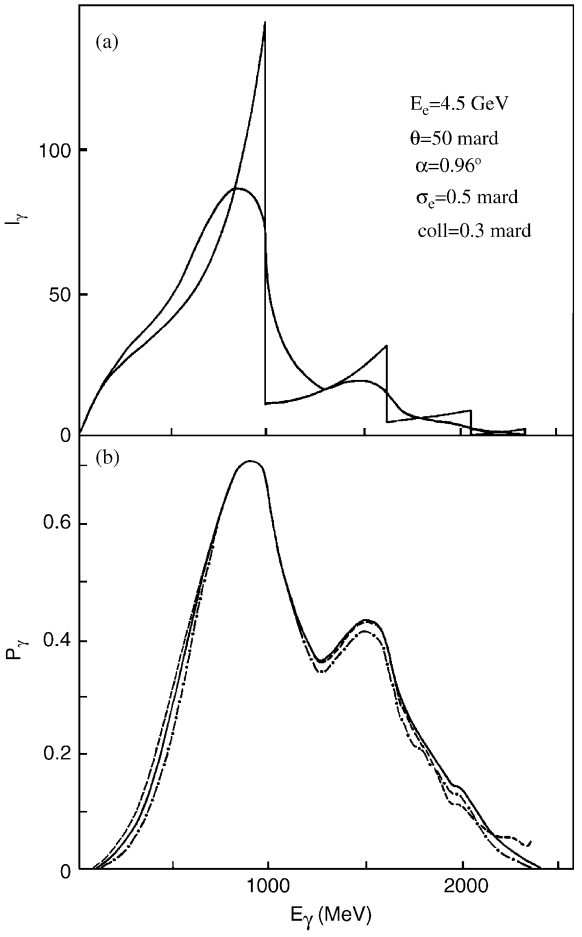

Fig. 2. (a) The part of the simulated CB intensity spectrum at $E_e = 4.5\,\text{GeV}$ and $x_{(0\,\bar{2}\,2)} = 0.22$ with the incoherent contamination subtracted. (b) The polarization spectra: MC (full curve), method 1 (dashed), method 2 (dot–dashed).

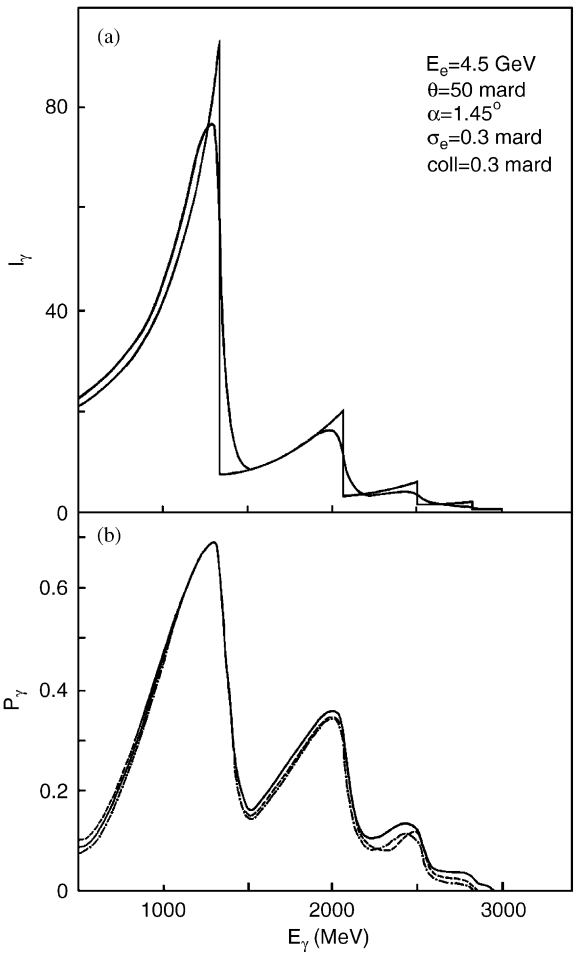

Fig. 3. The same as in Fig. 2 for $x_{(0\,\bar{2}\,2)} = 0.3$.

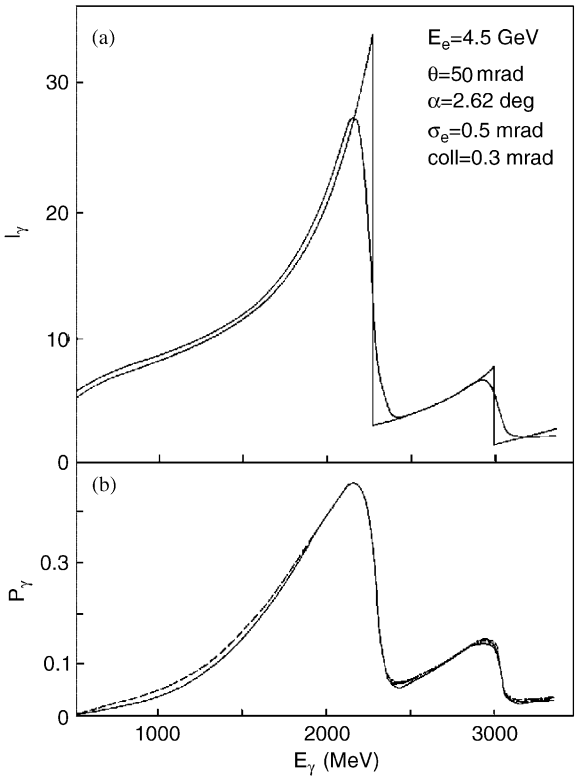

Fig. 4. The same as in Fig. 2 for $x_{(0\bar{2}2)} = 0.5$.

deviation from the MC data does not exceed 0.02–0.03 in the region of $\Delta x/x \leqslant 0.2$. In the case of the smaller collimation, method 2 reproduces the MC data for P with an accuracy 0.01–0.02 in the wide region ($\Delta x/x \leqslant 0.6$) of the peak energies $0.2 \leqslant x_{(0\bar{2}2)} \leqslant 0.5$.

We have investigated the several sources of the systematic uncertainties which have an impact on a polarization calculation:

6.1. Choice of the atomic form-factors

The AFFs enter into any CB polarimetry method which involve electromagnetic scattering from an atomic target as a whole. Analyses of experimental CB spectra for diamond and silicon crystals [4,13] have shown that Hartree–Fock (HF)-type form-factors give the best description of the data. However, improving the precision in the description of CB spectra may require further refinements to these form-factors, which are expected to be continuously improving on the basis of faster computers and advances in atomic theory. We have investigated the relative influence of the different AFF choice on the polarization calculated using CBSA methods. Fig. 5a shows the part of a CB intensity spectrum around $x_{(0\bar{2}2)} = 0.22$ measured by the 30 channel pair spectrometer [14] and the corresponding polarization spectra (Fig. 5c) obtained for a few selected AFF models: exponential, Molier, HF, Dirac-Slater wave functions-based HF, relativistic HF and the latest shell model-based HF one, respectively (see Ref. [15a–f]).

An important result of this study is the high degree of agreement between all polarization spectra in the region of $\Delta x/x \leqslant 0.6$ within the tolerance of $\leqslant 0.02$, which is also clearly confirmed in the plot of the differences $(P_i(x) - P_{\mathrm{D-T}}(x))$ (Fig. 5d), where $P_{\mathrm{D-T}}(x)$ is the result found using the Doyle–Turner AFF [15e]. The sensitivity to the choice of AFF becomes more noticeable on the right-hand side of the plots in Fig. 2. This may be interpreted as a dominance of the $(0\bar{2}2)$ lattice vector in the primary CB peak region and difference in the dependence of AFFs presented on the momentum transfer to the crystal, more pronounced for the higher-order lattice vectors.

As is seen from Fig. 5c the data obtained are divided into two groups by being closest each to the other. The first group involves exponential and Moliere AFFs while the second one contains the others. Similar results were also obtained for the CB peak 1 setting around $x_{0\bar{2}2} = 0.5$.

6.2. Uncertainty in the peak energy

By varying the $x_{(0\bar{2}2)}$ position within a range of 5–10% for the theoretical spectrum construction, we verified the method for sensitivity to errors in the crystal angle settings. This variation was chosen to be similar in size to the width of the smearing function and is immediately responding on a position shift of the smearing function spectrum. This shift, however, has no visible influence with an accuracy $\Delta P \leqslant 0.005$. The plot of the smearing function $W(x)$, superimposed by Gaussian fit, is shown in Fig. 5b extracted from the

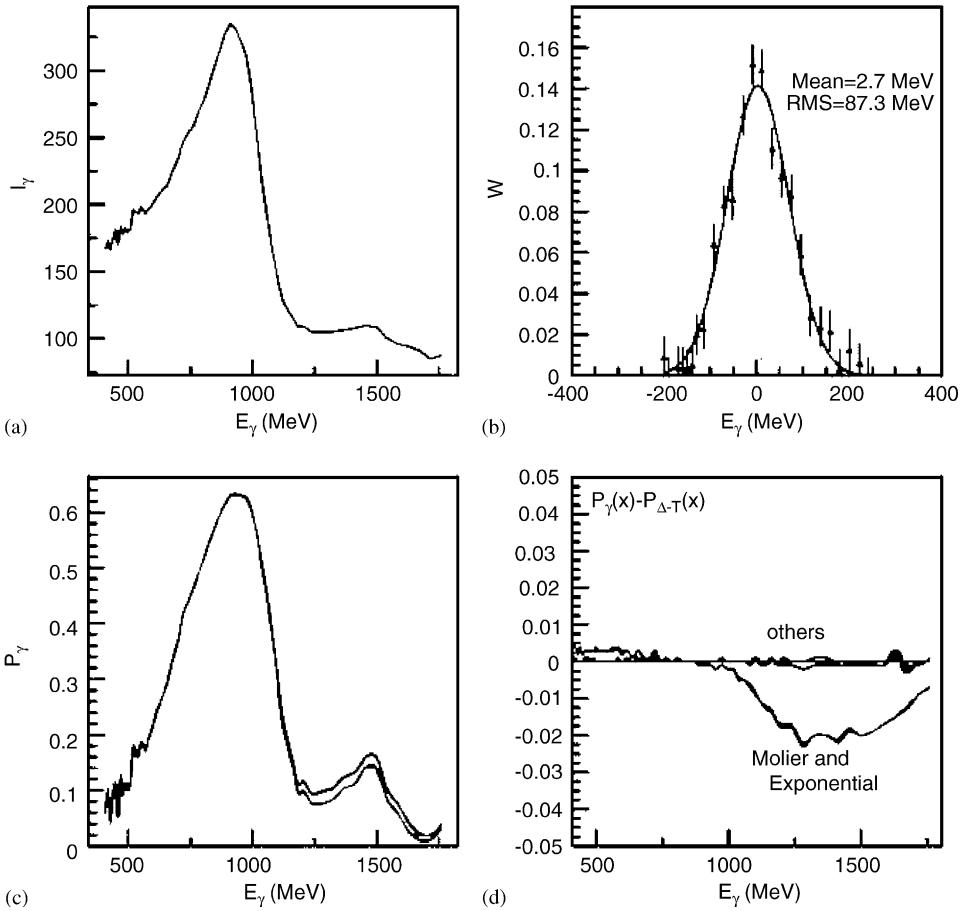

Fig. 5. (a) The part of the experimental CB spectrum for the $x_{(0\bar{2}2)} = 0.3$ and $E_e = 3350$ MeV. (b) The smearing function, fitted by Gaussian. (c) The results of the polarization calculations within method 1 for the AFFs noted. (d) The difference of the polarization data obtained with AFFs noted and Doyle–Turner's one [15f].

experimental spectrum (see Fig. 5a). As seen from the figure, $W(x)$ is centered satisfactorily close to zero, indicating the correctness of the value assigned to $x_{(0\bar{2}2)}$.

6.3. Choice of widths for the shape analysis regions

The widths of the integration regions used for the incoherent contamination correction were varied to verify for systematics in the subtraction procedure. Also, the size of the region used to extract the smearing function was varied, and the number of points used in the FFT was changed from 64 to 128. None of these variations resulted in changes in the polarization outside the tolerance $\Delta P \leqslant 0.005$.

6.4. Effects from smoothing

For this study, the statistical errors on the individual data points in the experimental spectrum were taken at the level of 5%. This statistical error is high compared to the usual case of the CB spectrum, but it presents a good test of smoothing because it leads to large oscillations in the extracted shape for $W(x)$ unless smoothing is applied. The results obtained show the possible effect of a coherent peak's shape, the most at its

maximum with suppression in the calculated polarization value up to 0.005, so this was applied in a region where the spectrum is relatively flat.

7. Conclusion

As one may conclude, CBSA methods of polarimetry are capable of determining beam polarization with a precision level of 0.01–0.02 within the investigated CB peak energy range $x_{(0\,\tilde{2}\,2)} = 0.2$–$0.5$. The extension of these techniques to larger values of x without loss in accuracy will require a more precise knowledge of the AFF of carbon than has been used in the past. One way of achieving this would be to measure the beam polarization at a CB source using a direct polarimetry method with a precision $\Delta P \leqslant 0.02$, and simultaneously measuring the CB energy spectrum [16].

Comparison between the direct and CBSA results will lead to improvements in the determination of AFF of carbon in the momentum range relevant to CBSA polarimetry. With this cross-check, we claim, in combination with a direct polarimetry technique, CBSA methods are an essential tool for any CB facility with a need for percent-level polarimetry.

Acknowledgements

This work has been supported by the CRDF grant AP2-2305-YE-02.

Appendix A

The CB's weighted intensity $I^{\mathrm{th}}(x,\theta,\alpha)$ relates to the bremmstrahlung cross-section $\mathrm{d}\sigma(x,\theta,\alpha)/\mathrm{d}x$ as

$$I^{\mathrm{th}}(x,\theta,\alpha) = x\,\mathrm{d}(\mathrm{d}\sigma(x,\theta,\alpha)/\mathrm{d}x \tag{A.1}$$

where $x = E_\gamma/E_{\mathrm{e}}$ is the ratio of the radiated photon energy to that of the incident electron, θ and α are the azimuthal and polar angles defined relative to the crystallographic axes as shown in Fig. 1a. The intensity I^{th} is defined as a sum of the coherent (I^{coh}) and incoherent (I^{inc}) components of CB spectrum:

$$I^{\mathrm{th}}(x,\theta,\alpha) = I^{\mathrm{coh}}(x,\theta,\alpha) + I^{\mathrm{inc}}(x), \tag{A.2}$$

$$I^{\mathrm{coh}}(x,\theta,\alpha) = [1+(1-x)^2]\,\psi_1^{\mathrm{c}}(x,\theta,\alpha) - (2/3)\,(1-x)\psi_2^{\mathrm{c}}(x,\theta,\alpha), \tag{A.3}$$

$$I^{\mathrm{inc}}(x) = [1+(1-x)^2]\psi_1^{\mathrm{inc}} - (2/3)\,(1-x)\psi_2^{\mathrm{inc}} \tag{A.4}$$

where the coherent structure functions $\psi_1^{\mathrm{c}}(x,\theta,\alpha)$ $\psi_2^{\mathrm{c}}(x,\theta,\alpha)$ are defined as:

$$\psi_1^{\mathrm{c}}(x,\theta,\alpha) = \frac{(2\pi)^2}{2a^3}\,\delta \sum_g |S(g)|^2 \mathrm{e}^{-Ag^2} F(g^2)\,\frac{g_2^2+g_3^2}{g_\parallel^2}, \tag{A.5}$$

$$\psi_2^{\mathrm{c}}(x,\theta,\alpha) = 3\frac{(2\pi)^2}{a^3}\,\delta^2 \sum_g |S(g)|^2\,\mathrm{e}^{-Ag^2} F(g^2) \times \frac{(g_2^2+g_3^2)(g_\parallel-\delta)}{g_\parallel^4}. \tag{A.6}$$

The incoherent structure functions $\psi_1^{\mathrm{inc}}(x)$, $\psi_2^{\mathrm{inc}}(x)$ depending on the momentum transfer to the atom, are described by different approximations [1].

The crystal lattice constant of diamond is denoted by $a = 922$ in units of the electron Compton wavelength, $\vec{g}$ is a vector belonging to the crystal reciprocal lattice, $g_\parallel = \sin(\theta)(g_2\cos\alpha + g_3\sin\alpha)$ is the projection of $\vec{g}$ on the direction of the incident electron, $\delta = (m_{\mathrm{e}}c^2/2E_{\mathrm{e}})x/(1-x)$ is the minimum momentum transfer allowed at a given value of x, $S(g)$ is the crystal structure factor, $A(g^2)$ is the Debeye–Waller factor and $F(g^2)$ is the AFF of carbon. The value for the linear polarization is expressed through a ratio of ψ_3^{c} structure function to the full intensity as

$$P^{\mathrm{th}}(x,\theta,\alpha) = \frac{2(1-x)\psi_3^{\mathrm{c}}(x,\theta,\alpha)}{I^{\mathrm{th}}(x,\theta,\alpha)} \tag{A.7}$$

where structure function ψ_3^{c} is written as a

$$\psi_3^{\mathrm{c}}(x,\theta,\alpha) = -\frac{(2\pi)^2}{a^3}\,\delta^3 \sum_g |S(g)|^2\,\mathrm{e}^{-Ag^2} F(g^2) \times \frac{[(g_2^2-g_3^2)\cos 2\alpha + 2g_2g_3\sin 2\alpha]}{g_\parallel^4}. \tag{A.8}$$

Eq. (A.8) For the definition of polarization, see Appendix B.

For the polarization calculation we also use a corrected expression in the place of Eq. (A.7):

$$P^{\mathrm{th}}(x,\theta,\alpha)=\frac{2(1-x)\psi_3^{\mathrm{c}}(x,\theta,\alpha)}{I^{\mathrm{coh}}(x,\theta,\alpha)}\,\frac{\beta}{\beta+1} \tag{A.9}$$

where $\beta = I^{\mathrm{coh}}/I^{\mathrm{inc}}$ is the ratio of the coherent to the incoherent CB components which can be adjusted to account for small incoherent contaminations.

Appendix B

The CB polarization is defined as

$$P^{\mathrm{th}}(x,\theta,\alpha)=\frac{I_{\perp}^{\mathrm{th}}-I_{\parallel}^{\mathrm{th}}}{I^{\mathrm{th}}}=\frac{I_{\perp}^{\mathrm{coh}}-I_{\parallel}^{\mathrm{coh}}}{I^{\mathrm{th}}} \tag{B.1}$$

where $I_{\perp}^{\mathrm{th}}$ and $I_{\parallel}^{\mathrm{th}}$ are the components of a radiation intensity ($I^{\mathrm{th}} = I_{\perp}^{\mathrm{th}} + I_{\parallel}^{\mathrm{th}}$) with the polarization vector perpendicular (parallel) to the plane $\vec{p}_{\mathrm{e}} \times \vec{b}_{\mathrm{l}}$ (see Fig. 1).

Each polarization component may be additionally decomposed into its coherent and incoherent parts:

$$I_{\perp,\parallel}^{\mathrm{th}} = I_{\perp,\parallel}^{\mathrm{coh}} + \tfrac{1}{2} I^{\mathrm{inc}}. \tag{B.2}$$

In analogy with the expression given in Eq. (B.1) one may define an experimental polarization as

$$P^{\mathrm{exp}}(x)=\frac{I_{\perp}^{\mathrm{exp}}-I_{\parallel}^{\mathrm{exp}}}{I^{\mathrm{exp}}} \tag{B.3}$$

where $I_{\perp}^{\mathrm{exp}}, I_{\parallel}^{\mathrm{exp}}$ are the components of experimental intensity $I^{\mathrm{exp}} = I_{\perp}^{\mathrm{exp}} + I_{\parallel}^{\mathrm{exp}}$, which can be expressed in terms of the theoretical ones according to a linear smearing operator as:

$$I_{\perp,\parallel}^{\mathrm{exp}}(x)=\int I_{\perp,\parallel}^{\mathrm{th}}(x,\theta,\alpha)\,W(\theta,\alpha)\,\mathrm{d}\theta\,\mathrm{d}\alpha. \tag{B.4}$$

With this definition and without use of a 'factorization' hypothesis [6,7] one may rewrite Eq. (B.3) as

$$P^{\mathrm{exp}}(x)=\frac{\int (I_{\perp}^{\mathrm{th}}-I_{\parallel}^{\mathrm{th}})W(\theta,\alpha)\,\mathrm{d}\theta\,\mathrm{d}\alpha}{I^{\mathrm{exp}}(x)}. \tag{B.5}$$

Taking into account Eq. (B.1) leads to the final expression:

$$P^{\mathrm{exp}}(x)=\frac{\int (P^{\mathrm{th}}(x,\theta,\alpha)\,I^{\mathrm{th}}(x,\theta,\alpha)\,W(\theta,\alpha)\,\mathrm{d}\theta\,\mathrm{d}\alpha}{I^{\mathrm{exp}}(x)}. \tag{B.6}$$

References

[1] M.L. Ter-Mikaelian, Zh. Eksp. Teor. Fiz. 25 (1953) 296; H. Uberall, Phys. Rev. 103 (1956) 1055; G. Bologna, et al., IL Nuov. Cim. A XLII (4) (1966) 844.
[2] V.D. Burkert, Proceedings of NSTAR-2001, Workshop on the Physics of Exited Nucleons, Mainz, 7–10 March 2001, P. 457.
[3] G. Diambrini-Palazzi, Rev. Mod. Phys. 40 (3) (1968) 611.
[4] L. Criegee, et al., Phys. Rev. Lett. 16 (1966) 1031.
[5] A. Kraus, et al., Phys. Rev. Lett. 79 (1997) 3834.
[6] U. Timm, Fortschr. Phys. 17 (1969) 765.
[7] J. Ahrens, in: Proceedings of Workshop "Polarized Photon Polarimetry", 2–8 June 1998, Newport News, VI, CLAS-Note(CEBAF), 98-018, p. 8.
[8] H. Hakobyan, et al., Preprint YERPHI-908(59)-86, 1986.
[9] L.Ya. Kolesnikov, et al., Ukr. Phys. J. 29 (1984) 1296.
[10] A.G. Sveshnikov, A.I. Tikhonov, Theory of Functions of Complex Variables, Nauka, Moscow, 1974.
[11] H. Hakobyan, G. Karapetyan, Preprint YERPHI-1138(15)-89, 1989.
[12] L. Rabiner, B. Gold, Theory and Application of Signals' Digital Processing, Mir, Moscow, 1978.
[13] I. Endo, et al., Phys. Rev. Lett. 60 (1988) 2292.
[14] F. Adamyan, et al., Eur. Phys. J. A 8 (2000) 423.
[15] (a) Y.S. Tsai, Rev. Mod. Phys. 46 4 1974 815
(b) E.A. Dahl, Preprint Bonn-IR-82-26, 1982
(c) D.T. Cromer, J.T. Waber., Acta. Crystallogr. A 18, 1968, 104
(d) D.T. Cromer, J.B. Mann., Acta. Crystallogr. A 24 1968, 321
(e) P.A. Doyle, P.S. Turner., Acta.Crystallogr. A 24 1968 390
(f) F.P. Korshunov, A.P. Lazar., Yad. Fiz. 66 2003 442
[16] F. Adamyan, et al., Nucl. Inst. and Meth. A 546 (2005) 376.